Cellulose (2024) 31:3699–3715
https://doi.org/10.1007/s10570-024-05802-2

ORIGINAL RESEARCH

Cellulose nanofiber/bio-polycarbonate composites as a transparent glazing material for carbon sequestration

Seul-A Park · Hyeonyeol Jeon · Min Jang · Semin Kim · Sung Yeon Hwang · Chae Hwan Hong · Jun Mo Koo · Dongyeop X. Oh · Jeyoung Park

Received: 4 September 2023 / Accepted: 12 February 2024 / Published online: 10 March 2024

Abstract Climate change, largely attributable to the extensive use of fossil fuels and deforestation, poses a critical global issue. There is a pressing need for innovative and sustainable solutions. This study highlights a significant advancement in materials science: a biomass-sourced transparent composite developed from cellulose nanofibers (CNFs) and isosorbide polycarbonates (ISB-PC). This green glazing material serves as a potential replacement for heavy, easily shattered glass in the construction and automotive industries, exhibiting remarkable thermal properties, light transmittance, and mechanical resilience. Notably, the thermal dimensional stability and transparency of the composite matches that of conventional glass. An integral accomplishment is the development of a multi-layered sheet with a thickness beyond 350 µm. These sheets achieved a light transmittance of 62.0% and coefficient of thermal expansion below 60 ppm K^{-1} (30–120 °C). Another distinguishing feature of this composite is its potential for carbon sequestration owing to its non-degradability. This study underscores the composite's potential as an eco-friendly alternative to glass.

Keywords Cellulose nanofiber · Bioplastic · Impregnation · Glazing plastic · Thermal dimensional stability

Supplementary Information The online version contains supplementary material available at https://doi.org/10.1007/s10570-024-05802-2.

S.-A. Park · H. Jeon · M. Jang · S. Kim · S. Y. Hwang · J. M. Koo · D. X. Oh · J. Park
Research Center for Bio-Based Chemistry, Korea Research Institute of Chemical Technology (KRICT), Ulsan 44429, Republic of Korea

S. Y. Hwang
Department of Plant and Environmental New Resources and Graduate School of Biotechnology, Kyung Hee University, Yongin-si 17104, Gyeonggi-do, Republic of Korea

C. H. Hong
Research and Development Division, Hyundai Motor Company, Uiwang-si 16082, Gyeonggi-do, Republic of Korea

J. M. Koo
Department of Organic Material Engineering, Chungnam National University, Daejeon 34134, Republic of Korea

D. X. Oh (✉)
Department of Polymer Science and Engineering and Program in Environmental and Polymer Engineering, Inha University, Incheon 22212, Republic of Korea
e-mail: d.oh@inha.ac.kr

J. Park (✉)
Department of Chemical and Biomolecular Engineering, Sogang University, Seoul 04107, Republic of Korea
e-mail: jeypark@sogang.ac.kr

Introduction

Human-induced global warming, propelled by greenhouse gas (GHG) emissions, poses a severe hazard to humans. Annually, approximately 36–40 billion metric tons of carbon dioxide (CO_2) are emitted, primarily from fossil fuel consumption and deforestation (Liu et al. 2022). The consequent increases in temperature and sea level have caused climate disruption, natural disasters, and the extinction of numerous species (Ceballos et al. 2020; Zhu and Fan 2021; Iossifidis and Garforth 2022; Lindsey and Dahlman 2023), demanding urgent and sustained action to curtail carbon emissions.

Metals and ceramics are primarily used in the automotive and construction industries; however, their production and processing demand substantial energy and generate high carbon emissions (Hertwich 2021; Ren et al. 2021; Vanderreydt et al. 2021; Zhang et al. 2021). A viable strategy to reduce carbon emissions relies on replacing these metals with ceramics or plastic materials (Furszyfer Del Rio et al. 2022; Raabe 2023). Furthermore, lightweight plastic components in vehicles notably enhance energy efficiency (Czerwinski 2021).

Carbon capture, utilization, and storage (CCUS) offers promising potential in carbon emission reduction. However, this technology faces several limitations that need to be addressed (Marocco Stuardi et al. 2019; Quarton and Samsatli 2020; Ra et al. 2020; Becattini et al. 2021; Chen et al. 2022; Gür 2022). A key challenge is the energy-intensive process of separating and capturing CO_2 using membranes as adsorbents (Pfister et al. 2017; Chen et al. 2020). This process requires a significant amount of energy and incurs high costs, which hinder its large-scale implementation (Labaran et al. 2022; Vaz et al. 2022). In addition, stored CO_2 may leak owing to geological factors such as seismic activity (Arora et al. 2019; Song et al. 2023). This poses severe risks to the environment and public safety, highlighting the need for effective, secure, and reliable storage solutions. Another challenge with CCUS is the low efficiency of storing CO_2 as calcium carbonate ($CaCO_3$) owing to the weight of calcium and oxygen involved in the process (Czaplicka et al. 2020; Leonzio et al. 2020). This limits the amount of CO_2 that can be stored, thereby hindering achievement of the desired reduction in carbon emissions.

Biomass-derived plastics have the potential to be used as CCUS materials in high-carbon-content stable solids rather than CO_2 or $CaCO_3$; this is particularly true in automotive and construction applications (Motagamwala et al. 2018; Koo et al. 2020; Wang et al. 2021; Hong 2022; Chung et al. 2023; Jung et al. 2023). Terrestrial vegetation captures approximately 120 Gt CO_2 annually through photosynthesis, which is more than three times the amount generated by human activities (Majumdar and Deutch 2018). The utilization of biomass-derived plastics as semi-permanent structural materials can contribute to carbon sequestration. Stegmann et al. conjectured that recycling or sequestering biomass feedstock plastics in landfills could generate medium- or long-term carbon sinks (Stegmann et al. 2022). Theoretically, 275 Gt of negative carbon emissions can be sequestered into 75 Gt of biogenic carbon from nonbiodegradable bio-based plastics. This study recommended that employing such strategies could contribute to a 75% global temperature reduction by 1.5 °C until 2100. The emergence of trees during the Paleozoic Carboniferous Period signified a crucial evolutionary milestone because the absence of cellulose-/lignin-digesting microbes reduced atmospheric CO_2 and induced climate cooling (Kenrick and Crane 1997; Cleal and Thomas 2005). Recently, wooden buildings have become increasingly popular in contemporary architecture and design as a sustainable and environmentally friendly alternative to conventional materials, such as concrete and steel (Ramage et al. 2017). The two prominent firms that have incorporated wood into their building designs are SOM and 3XN. One project undertaken by SOM was the Green School in Bali, Indonesia, where the entire campus was made of bamboo; the campus also features open-air classrooms and sustainable energy systems (Vanderbilt 2017). 3XN undertook the construction of the University of Arkansas Adohi Hall, a student housing project in Fayetteville that features cross-laminated timber construction (Prevost 2023).

Glazing plastics, including bio-based variants, are considered sustainable alternatives to glass for window construction owing to their lower density and higher viscoelasticity (Hauenstein et al. 2017). Glass represents a large portion of building construction and automobile components. Transparent polycarbonates, with a density of 1.2 g cm^{-3}, are less vulnerable to shattering and possess half the

density of glass. However, their limited thermal stability has hindered their widespread adoption in automobile windshields and sunroofs (Chauhan et al. 2022). Glass exhibits a coefficient of thermal expansion (CTE) of 3–9 ppm K^{-1} at 20 °C, whereas polycarbonates demonstrate a significantly higher CTE of 65–70 ppm K^{-1}; further, biopolymers are susceptible to hydrolysis and biodegradation. The aforementioned aspects render these materials unsuitable as structural materials (Vieira et al. 2011; Kim et al. 2021a, 2021b).

Hierarchical wood structures facilitate the design and fabrication of advanced polymer composites with excellent mechanical properties (Lee et al. 2014; Guo et al. 2022; Pashazadeh et al. 2023; Solikhin et al. 2023). The constituent cellulose nanofibers (CNFs) of plant cell walls exhibit a low CTE of approximately 2 ppm K^{-1} (Nogi and Yano 2008; Li et al. 2018; Nguyen et al. 2021; Tanpichai et al. 2022; Jeon et al. 2023; Qi et al. 2023). In particular, bacterial CNFs exhibit high chemical purity and good moldability, which are useful for lamination applications (Guan et al. 2020a, 2020b, 2021a; Ludwicka et al. 2020). Lignin is a highly crosslinked polymer that provides structural support and imparts rigidity and stability to wood (Kim et al. 2011).

In this study, we endeavor to address the pressing global issue of climate change by developing a transparent biomass-sourced composite material with exceptional thermal and dimensional stabilities. Inspired by the hierarchical structure of wood and utilizing CNFs as a structural framework combined with isosorbide-based polycarbonates (ISB-PCs), we created a nonbiodegradable and transparent plastic composite that exhibits remarkable thermal and dimensional stabilities, while offering the potential for carbon sequestration (Fig. 1). The innovative design of our composite aims to overcome the limitations of conventional cellulose-based materials and contribute to sustainable solutions for transportation and building construction. In contrast to conventional cellulose-based materials, this non-biodegradable composite exhibits superior thermal properties, rendering it suitable for mid- to long-term transportation and building construction applications. Over 80 wt.% of the composite material consists of biogenic carbon, which effectively functions as a carbon storage solution. Our innovative design employs a pre-impregnated nanocomposite comprising a CNF film as the

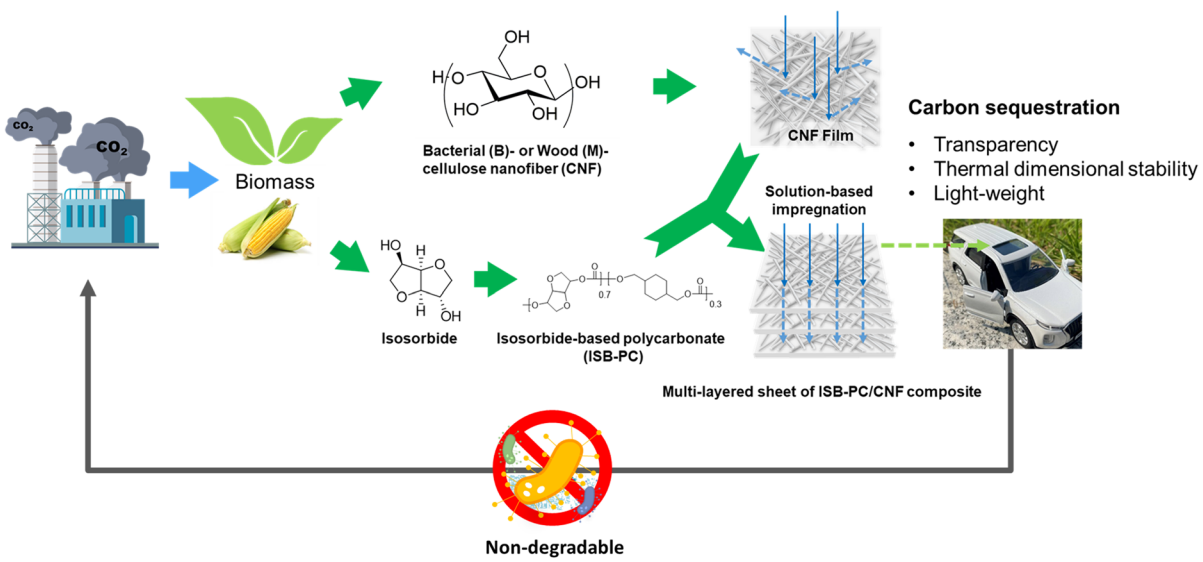

Fig. 1 Transparent plastic composite with exceptional thermal and dimensional stabilities comprising cellulose nanofibers (CNFs) and isosorbide-based polycarbonate (ISB-PC), prepared using a pre-impregnation method. The composite material is proposed as a transparent glass material for automobile and construction applications owing to its superior performance characteristics. It can also serve as a carbon storage material, contributing to carbon capture utilization and storage (CCUS) efforts owing to its nondegradable properties

structural framework; ISB-PCs are impregnated into the pores of the framework. ISB is a bioderived alicyclic ring monomer that can impart remarkable thermophysical and optical properties to polymers (in addition to significant UV resistance) owing to its chromophore-free characteristics. In contrast to conventional carbon-based nanoparticles, which exhibit a low CTE of less than 50 ppm K^{-1} but are restricted by their dark color, chromophore-free CNFs display a density similar to that of conventional polymers (Xu et al. 2011; Ji et al. 2016; Yano et al. 2018; Kim et al. 2020; Guan et al. 2021b).

Experimental

Reagents and materials

ISB (99.8% purity) was supplied by Roquette Frères (France) and used after recrystallization from acetone. 1,4-cyclohexanedimethanol (CHDM 99.5%) with 74 mol% trans-isomer was supplied by SKC, Inc. (Korea). Triphenylphosphite (TPP, 97%), 2,6-di-tert-butyl-4-hydroxymethylphenol (DBHP, 97%), tetramethylammonium hydroxide (TMAH, 97%), diphenyl carbonate (DPC, 99%), and poly(bisphenol-A carbonate) (BPA-PC, average M_w of 45,000 g/mol) were purchased from Sigma-Aldrich (USA) and used without further purification. *N*,*N*-dimethylacetamide (DMAc) (HPLC reagent grade, 99.8%) used for impregnation was purchased from Samchun Pure Chemicals (Korea). Bacterial cellulose nanofiber sheets (B-CNFs) produced by natural fermentation methods were purchased from Briskin Inc. (Korea) (Jo 2013; Qian et al. 2023). Mechanically exfoliated cellulose nanofibers (M-CNFs) in an aqueous slurry (3.1 wt%, with 90% fine grade, Lot#U35) were obtained from the University of Maine Process Development Center (USA). CNFs have a diameter of ~ 50 nm and a length of up to a few micrometers.

Preparation of ISB-PC

ISB-PC ([ISB]: [CHDM] molar ratio = 70:30) was polymerized as described in our previous study (Park et al. 2017). ISB (29.81 g, 0.204 mol), CHDM (12.61 g, 0.087 mol), and DPC (62.43 g, 0.291 mol) were added to a 300 ml dried glass vessel to attain the target yield of 50 g. TMAH (100 mg, 0.55 mmol) (as a catalyst) and TPP (100 mg, 0.32 mmol) and DBHP (100 mg, 0.42 mmol) (as thermo-stabilizers) were added. The reactor was heated gradually in an oil bath at 150 °C for 2 h under a N_2 atmosphere. The temperature was increased to 180 °C, and the pressure was reduced gradually from 100 to 30 Torr over 2 h to distill off phenol (byproduct). Then, the temperature was increased gradually to 240 °C, and the pressure was reduced gradually to < 0.05 torr. Polymerization was terminated after 30 min. The final polymer products (49 g, 98%) were collected after the pressure was returned to ambient conditions using a nitrogen purge. M_n: 62,300 g mol^{-1}, PDI: 1.91, and T_g: 130 °C. ^{1}H nuclear magnetic resonance (^{1}H NMR) spectroscopy ($CDCl_3$, 600 MHz, ppm): 5.10–5.08, 4.89, 4.56–4.54, 4.07–3.91, 1.90–1.83, 1.66–1.57, 1.43, 1.02.

Preparation of M-CNF film

CNF films were prepared using a simple solution-casting method. The 3.1 wt.% stock solution of CNFs was diluted to 0.5% with deionized water and stirred using a homogenizer (IKA T25 digital Ultra-Turrax, Germany) at 12 krpm for 10 min. Subsequently, the CNF solution was poured into a petri dish (Ø 150 mm) and dried under ambient conditions for seven days. The formed CNF film was then removed from the petri dish to obtain ~ 40 µm-thick films.

Preparation of B-CNF film

Contaminants from the surface of the B-CNF sheet were removed by washing the sheet several times with deionized water and soaking the flattened sheet on a tray containing ethanol for 1.5 h. Then, the sheet was removed from the tray, placed on a polypropylene film, and dried in an oven at 40 °C for 24 h to obtain the final neat B-CNF film.

Preparation of polycarbonate-impregnated nanocellulose film and multi-layered sheet

ISB-PC polymer solutions were prepared by dissolving 10 wt.% polymers in DMAc. Nanocellulose films (M-CNFs and B-CNFs, 3 cm × 3 cm) were soaked in the polymer solutions at ambient temperature for 1 h for impregnation. The impregnated nanocellulose films were transferred to a glass petri dish (Ø 50 mm) filled with 3 mL of ISB-PC polymer solution.

These were then dried in an oven at 80 °C for 24 h (M-CNF-1 and B-CNF-1). To prepare the multilayered sheets, the impregnation process was conducted in a similar manner by stacking three or six layers of nanocellulose films (M-CNF-3, M-CNF-6; and B-CNF-3, B-CNF-6).

Characterization

^{1}H NMR spectra were acquired using a Bruker AVANCE spectrometer (Avance NEO 600, Bruker, USA) at a proton frequency of 600 MHz. The samples were dissolved in $CDCl_3$ containing 0.03 vol% tetramethylsilane as an internal standard. The [ISB]:[CHDM] molar ratio of neat ISB-PC was determined using ^{1}H NMR spectroscopy (Park et al. 2017). Within the ^{1}H NMR spectrum, the peaks observed at δ 5.1–4.5 ppm correspond to the 4 hydrogen atoms of ISB, whereas those around 4.1–3.8 ppm represent the 4 hydrogen atoms of ISB and 4 hydrogen atoms of CHDM. Consequently, the molar content of ISB in the copolycarbonates was calculated based on the integral intensity ratio between 5.1 ppm and 3.8 ppm (Fig. S1).

The number-average molecular weight (M_n), weight-average molecular weight (M_w), and polydispersity index (PDI = M_w/M_n) were measured using gel permeation chromatography (GPC) with an ACQUITY APCXT column (Waters Corp., USA) at 40 °C and a refractive index detector using chloroform as the mobile phase. The system was universally calibrated using polystyrene standards. The M_n, M_w, and PDI of neat ISB-PC were characterized by GPC.

Differential scanning calorimetry (DSC 25, TA Instruments, USA) was performed in the range 30–180 °C, at heating and cooling rates of 10 °C min^{-1} under a nitrogen atmosphere.

The transparency of the film was measured using an ultraviolet–visible (UV/VIS) spectrometer (UV-2600, Shimadzu Corp., Japan) in the wavelength range 400–800 nm.

The CTE of the film was evaluated via thermomechanical analysis (TMA-Q 400, TA Instrument, USA) in a nitrogen atmosphere over the temperature range 25–200 °C, under 10 °C min^{-1} heating and cooling rates, and a probe force of 20 mN. The length and width of the TMA specimens were 30 and 5 mm, respectively.

The surface and cross-sectional morphologies of the sample films were observed using field-emission scanning electron microscopy (FE-SEM) (SU-8220, Hitachi, Japan) at an accelerating voltage of 5 kHz. Prior to the SEM measurements, the samples were coated with a thin platinum alloy using a sputter coater (K575X, Emitech, UK) under vacuum to reduce charge interruptions.

The mechanical properties were measured by a universal testing machine (UTM) (Instron 5943, USA) at 25 °C using a load cell of 1 kN and crosshead speed of 10 mm min^{-1} (i.e., 100% min^{-1} as strain notation). The specimens used for UTM testing were cut into a dog-bone shape using a cutting die in accordance with the ASTM D 638 Type V Standard (length and width of 63.5 and 9.53 mm, respectively).

The scratch resistance of the film was evaluated through pencil hardness tests using an SJTM-108MD (SAM JEE TECHNOLOGY, Korea) testing device in accordance with the guidelines of ASTM Standard D3360-00. A nano-indentation tester (TTX-NHT3, Anton Paar, Austria) was used to measure the surface mechanical properties of the films (Choi et al. 2023). The maximum load used, maximum load holding time, and both loading and unloading speeds were 10 mN, 30 s, and 10 mN s^{-1}, respectively.

The hydrophilicity of the film was evaluated through static water-contact angle tests at 25 °C using a contact angle goniometer (DSA 25, Kruss GmbH, Germany). The drop volume used for the measurement was 5 μL. The sessile drop method was used, in which a water drop was placed on the film surface and the contact angle of the water was measured. The dimensional change rate of the film corresponding to moisture absorption was measured using a thermomechanical analyzer (Discovery TMA450 RH, TA instruments, USA) employing a 50 mN probe force at 30 °C, and under a relative humidity of 40 − 60%. For the dimensional change rate measurements, the RH was gradually increased by 1% per 1-min intervals. In addition, a simplified experiment was designed to observe water resistance. The film was cut into squares of 1 cm × 1 cm and exposed to distilled water at 30 °C for 24 h to observe appearance changes on its surface, as well as to compare weight changes before and after exposure.

UV aging tests were performed using an ultraviolet-ozone (UVO) chamber (Model No. AC-6, AhTech LTS, Korea). The film was exposed for 30 min to

30 °C of temperature, 184/254 nm of wavelength, and 26 MW cm^{-2} of intensity. The changes in the transmittance of the films were compared before and after exposure.

Composting degradation experiments

The composting capabilities of the CNF/ISB-PC composite films were examined by embedding the film samples in conventional composting piles for 36 weeks using a mixture of fallen leaves, ground coffee, and straw as the compost. The carbon-to-nitrogen ratio (C:N) was maintained at 31.63. The acidity (pH 5–6), relative humidity (40–60%), and temperature (50–60 °C) were monitored continuously during the experiment. The composting conditions were aligned with the ISO 16929 Standard (Lim et al. 2023). For comparison, a B-CNF film made purely of cellulose, the reference material for ISO 16929, was fully degraded within a six-week period. The biodegradability of the CNF/ISB-PC composite films was evaluated based on weight loss.

Results and discussion

ISB-PC-impregnated CNF nanocomposite film: Sample preparation and characterization

By using an impregnation method with CNF film and ISB-PC (Fig. 2a), we developed a transparent glazing plastic. The process comprised four stages: (1) fabrication of a porous CNF film as a prepreg material, (2) synthesis of bio-polycarbonate, (3) infiltration of the

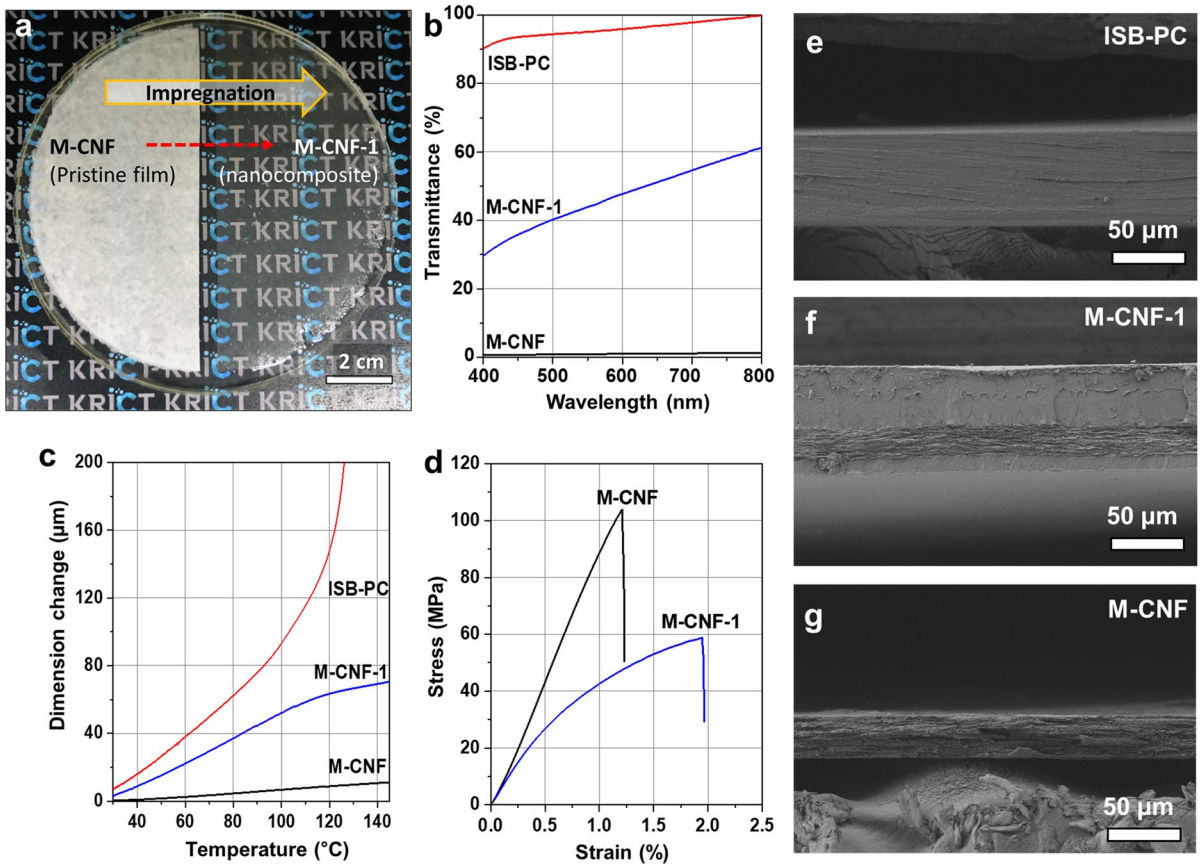

Fig. 2 Pre-impregnation method used for composite preparation. **a** Wood-derived cellulose nanofibers (M-CNFs) with and without the ISB-PC infiltration. **b, c** Visible ray transmittance vs. wavelength and dimensional variation vs. temperature curves, respectively, for M-CNFs, M-CNF/ISB-PC composite (M-CNF-1), and neat ISB-PC. **d** Tensile stress and strain curves of M-CNFs and M-CNF-1. **e–g** SEM images of tensile-fractured surfaces of ISB-PC, M-CNF-1, and M-CNFs

bio-polycarbonate solution into the porous CNF film, and (4) lamination of composite films to achieve the desired thickness.

Initially, two types of porous CNF films were prepared as prepregs: bacterial cellulose nanofibers (B-CNFs) (Wu et al. 2021) and wood-derived cellulose nanofibers prepared using the mechanical exfoliation method (M-CNFs) (Zhang et al. 2023). B-CNFs were generated via a fermentation process wherein bacteria formed dense, hydrogel-like CNF scaffolds in an aqueous nutrient medium according to the shape of the container. Purified B-CNFs, with the bacterial bodies removed, were used for this process. The B-CNF film in the form of hydrogel-like CNF scaffolds was produced by microbial fermentation. The aqueous medium in which it was cultured was replaced with ethanol because when removed from water and dried directly, the shape was distorted. Conversely, the purification of the never-dried wood pulp sludge was followed by water dispersion of the CNFs using a homogenizer. An aqueous CNF solution (3.05 wt.%) was purchased from the University of Maine and mixed with water to a 0.5 wt.% ratio. Subsequently, the aqueous CNF solution was dried to obtain the film. The B-CNF and M-CNF films exhibited thicknesses of approximately ~ 17 and ~ 40 µm, respectively. The transparency of both films was below 1% owing to the light scattering caused by the porous structure.

Subsequently, ISB-PCs were synthesized in the form of copolymers via a melt polycondensation process using two distinct diol monomers (ISB and CHDM) and DPC as the carbonate source. ISB-only homopolycarbonates tend to have low molecular weights, thus yielding brittle plastics. The incorporation of diverse diols enhanced the molecular weight and mechanical properties of the ISB-based copolycarbonates. CHDM, an alicyclic diol, was selected as the co-monomer for the ISB-based copolycarbonates because it augments the impact-related physical attributes of the final polymer and imparts ductility without compromising thermal stability. TMAH was used as a basic organic catalyst for the transesterification reaction. The copolycarbonates were synthesized at a molar ratio of [ISB]:[CHDM] = 70:30. According to a previous study (Park et al. 2017), the ISB-PC achieved the highest toughness at this optimal ratio. The ISB content calculated using ^{1}H NMR spectroscopy indicated a biogenic carbon percentage in ISB-PC exceeding 68 wt.%.

A unit film of the transparent composite was fabricated through a process that involved the immersion of the B-CNF film in alcohol or M-CNF film in a 10 wt.% ISB-PC/DMAc solution for 1 h. Post-dipping, the excess solution was removed, and the films were dried at 80 °C for 24 h. The single layers of B-CNF and M-CNF/ISB-PC composites were designated as B-CNF-1 and M-CNF-1, respectively. For illustrative purposes, M-CNF-1's characteristics are illustrated in detail in Fig. 2b–d. Significantly, the M-CNFs exhibited a light transmittance of 0.9% at 550 nm, whereas the M-CNF-1 composite exhibited a significant increase in light transmittance, reaching 43.9% at the same wavelength. This improvement in transparency resulted from the filling of empty spaces within the CNFs, which originally caused light scattering by the polymer.

In terms of thermal characteristics, M-CNF-1 exhibited a CTE of 39.85 ppm K^{-1} within the temperature range of 30–120 °C. This was significantly lower than those of neat ISB-PC (97.21 ppm K^{-1}) and BPA-PC (79.49 ppm K^{-1}). The mechanical properties of the M-CNF-1, neat M-CNFs, and PC were evaluated. The tensile properties of M-CNF-1 showed a remarkable balance, exhibiting a performance between those of neat ISB-PC and CNFs (Fig. 2c, Tables S1 and S2). M-CNF-1 displayed higher elongation (2.0%) and toughness (0.81 MJ m^{-3}) compared with those of neat CNFs; however, its Young's modulus (6.3 GPa) and tensile strength (62 MPa) were lower. In contrast, the elongation, toughness, Young's modulus, and tensile strength of neat CNFs were 1.2%, 0.64 MJ m^{-3}, 9.9 GPa, and 104 MPa, respectively. M-CNF-1 exhibited higher rigidity and hardness than ISB-PC and BPA-PC. Remarkably, its performance exceeded that of BPA-PC (a material conventionally used as a glass substitute in structures such as aquariums) for all parameters assessed. BPA-PC had a Young's modulus of 1.7 GPa, tensile strength of 67 MPa, and toughness of 29 MJ m^{-3} (Park et al. 2019a). The tensile-fractured surfaces of the tested specimens confirmed the simultaneous presence of ISB-PC and M-CNFs in the M-CNF-1 composite. More importantly, as ISB-PC became well impregnated into M-CNFs, balanced properties between the plastic and nanofiber sheets were observed (Fig. 2e–g).

Visible ray transmittance characteristics of CNF nanocomposite film

To enhance the suitability of the film for demanding glass applications, such as sunroofs (which require thicknesses beyond the submillimeter level), we prepared multilayered sheets by stacking several layers of impregnated films (Fig. 3). For the M-CNF series, the transmittance of an individually impregnated film at 550 nm decreased to 24.4% under a three-layer structure. Subsequently, it decreased to 15.1% under a six-layer configuration, owing to the increased thickness. The thicknesses of the one-layered, three-layered, and six-layered sheets (i.e., M-CNF-1) were 123 ± 16.0, 290 ± 15.3, and, 364 ± 15.5 µm, respectively, with M-CNF contents of 11.8 ± 0.7, 18.7 ± 0.5, and 23.3 ± 0.8 wt%, respectively (Table S3). Given the weight ratio of the CNFs, the biogenic carbon content in these composites was approximately 80 wt.%, resulting from the 68% theoretical biogenic carbon content of ISB PC, according to the ^{1}H NMR analysis. In view of these results, this particular composite could potentially function as a carbon storage solution. Considering that the carbon contents of carbon dioxide and calcium carbonate are 27 wt.% and 12 wt.%, respectively, the biogenic carbon sequestration efficiency of the composites is significantly high. Nevertheless, a more comprehensive validation of this hypothesis necessitates a life-cycle assessment (LCA) study of the factors in the carbon footprint associated with the production of CNF/ISB-PC composites (Benavides et al. 2020). In the context of an LCA, petrochemical polyethylene (PE) exhibits a carbon emission margin of 2.6 kg-CO_2 kg-plastic^{-1}, whereas bio-PE demonstrates a carbon emission margin of -1.0 kg-CO_2 kg-plastic^{-1}. This disparity arises from the low production energy requirements of bio-PE and its ability to resist degradation, which

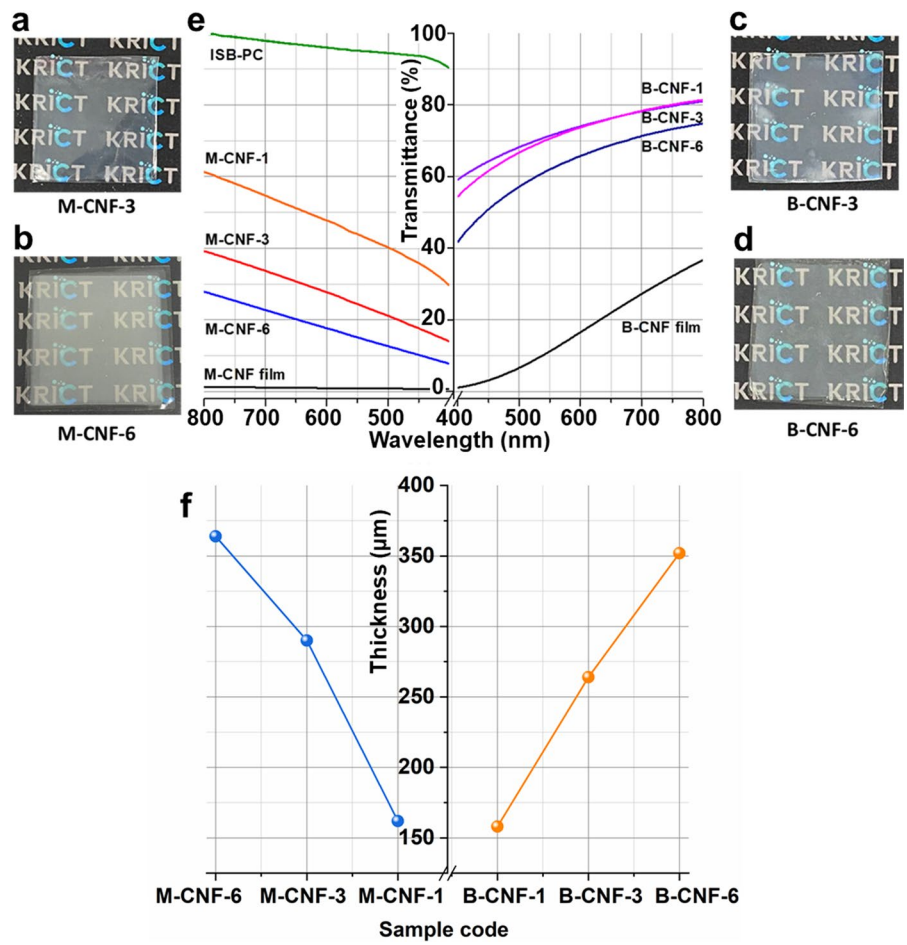

Fig. 3 Photographic images and visible ray transmittance curves of multi-layered M-CNF/B-CNF composite sheets. Photo-images of: **a** M-CNF-3, **b** M-CNF-6, **c** B-CNF-3, and **d** B-CNF-6 composite sheets (sheet size: 3 cm × 3 cm). **e** Visible ray transmittance and **f** thickness of M-CNF/B-CNF composite sheets depending on the number of layers

can lead to carbon sequestration. To fully actualize our proposed assumptions, it is imperative to conduct additional research aimed at reducing the production energy, particularly if the aim is to facilitate mass production of this composite.

The thicknesses of B-CNF-1, B-CNF-3, and B-CNF-6 were approximately 158 ± 7.0, 264 ± 7.2, and 352 ± 9.7 μm, respectively, and their CNF contents were 5.5 ± 0.5, 11.7 ± 0.6, and 20.3 ± 0.5 wt%, respectively. The B-CNF composite exhibited a significant increase in transparency after infiltration, with the single-layer impregnated film showcasing the highest transmittance of 71.4% at 550 nm. The three- and six-layered configurations showed transmittances of 70.6% and 62.0%, respectively, overall showcasing considerable levels of transmittance. Although the disparity in thickness may straightforwardly explain the higher transparency of the B-CNF composite (notwithstanding thickness variations of less than 15%), this factor alone appears insufficient when considering the principles of the Beer–Lambert equation (where the light transmittance is linearly correlated with $(\text{thickness})^{-1}$). Considering the substantial discrepancy in light transmittance (between 30 and 50%), additional factors to differences in thickness require examination to account for this phenomenon. Even with the naked eye, the transparency of the multilayered sheet made from B-CNFs was significantly higher, possibly stemming from the degree of nanofiber disintegration in the B-CNF and M-CNF precursors. In the case of M-CNFs, a drying process is necessary to obtain a fixed precursor; this, however, induces nanofiber aggregation. Conversely, B-CNFs display inherent freestanding properties (in the form of a hydrogel), thus enabling their immediate use after solvent exchange with alcohol without drying, thereby preventing aggregation (Hanif et al. 2017).

In contrast to industrial plastics, which often include antioxidants or fluorescent brighteners, a yellow tint manifests in the majority of lab-grade plastics during melting (Kucherov et al. 2017). This yellowing effect was also observed in the prepared CNF composites post heat treatment. In a previous study, no noticeable changes in the molecular weight or chemical structure of neat ISB-PC were observed after exposure to a temperature of 240 °C for 5 min (Park et al. 2017). Any potential reduction in molecular weight from β-hydrogen elimination at 240 °C was deemed insignificant. Therefore, the color alterations of the composites resulting from heat treatment had no significant impact on their mechanical properties.

Morphology and thermal stability characteristics of the multi-layered CNF composite sheets

The assessment of the thermal and dimensional stabilities and morphologies of the CNF/ISB-PC composites are illustrated in Fig. 4 and Table S4. Conventional bulk glass has a CTE of 41–54 ppm K^{-1} at 20–100 °C (Bogdanov et al. 2011), whereas thermosets exhibit a CTE > 50 ppm K^{-1} under similar temperature conditions (Park et al. 2019b). Here, the neat ISB-PC and BPA-PC samples displayed CTEs of 68.5 ppm K^{-1} and 71.6 ppm K^{-1}, respectively, at 30–80 °C. The corresponding values at 80–120 °C were 133.1 ppm K^{-1} and 89.4 ppm K^{-1}, respectively. Consequently, in the absence of reinforcing fillers, the PC series did not meet the thermal dimensional stability requirements for industrial-grade glass. As such, they are frequently reinforced with fiberglass when used as glass substitutes.

Notably, the CNF/ISB-PC composites achieved a remarkably low CTE (< ~ 50 ppm K^{-1}) at both low (30–80 °C) and high (80–120 °C) temperatures. Although the CTE values varied without a distinct pattern based on the number of layers and CNF type (M-CNF/B-CNF), probably owing to the interlayer voids, the highest CTE remained below 60 ppm K^{-1} across both temperature ranges. This result indicates that multilayered laminate structures can attain remarkable dimensional stability, equivalent to that of glass.

Given that automobile exteriors can reach temperatures up to 100 °C due to midsummer heat, the capability to suppress thermal expansion at high temperatures is crucial. The dimensional variation of 1 m of our glass-replacement plastics remained below 60 μm (Fig. 4e) even when the temperature was increased to 150 °C (which exceeds the glass transition temperature of ISB-PC (130 °C)); this demonstrates their notable anti-thermal expansion potential.

The distinctions observed in the cross-sectional SEM images (Fig. 4a–d) explain the higher transmittance of the B-CNF series compared to that of the M-CNF series. A detailed examination of the neat CNF top-surface reveals widely distributed fibers of diameters 58.0 ± 19.0 nm, and irregularly distributed pores of sizes 96.0 ± 50.6 nm in M-CNFs.

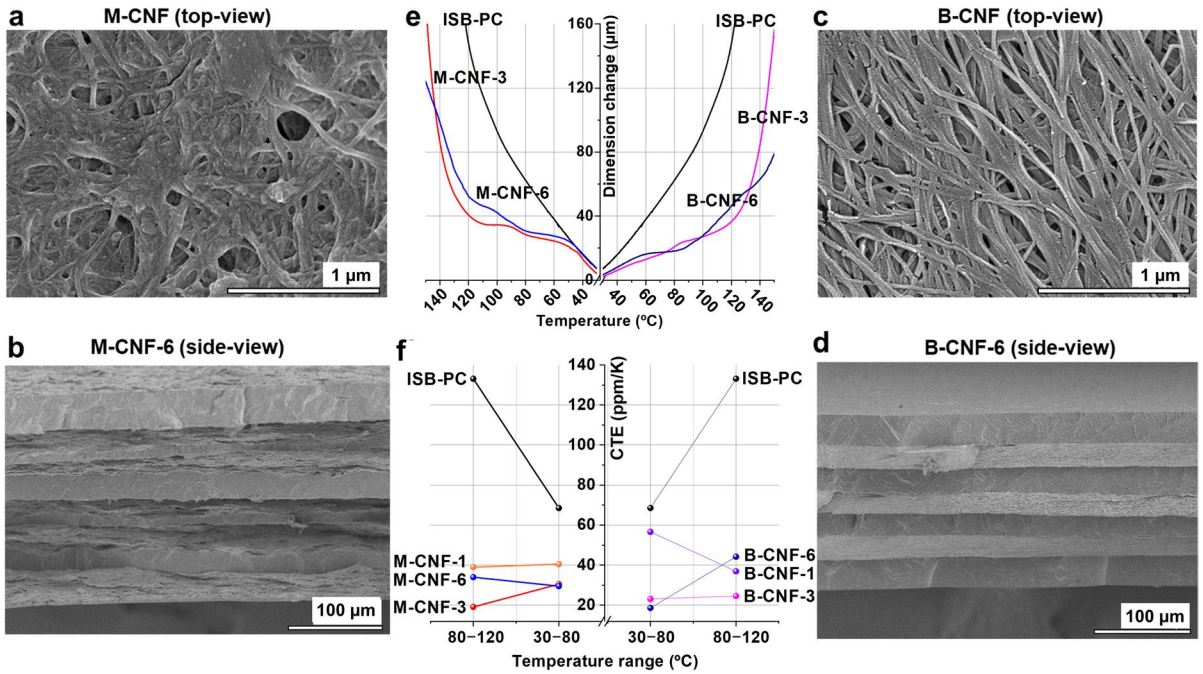

Fig. 4 Morphologies and thermal dimensional stabilities of multi-layered M-CNF/B-CNF composite sheets. SEM images of **a** neat M-CNF top-surface, **b** side-view of M-CNF-6, **c** neat B-CNF top-surface, and **d** side-view of B-CNF-6. **e** Temperature vs. dimensional variation curves, and **f** CTE values of M-CNF/B-CNF composite sheets depending on the number of layers

Conversely, B-CNF featured a uniform fiber diameter of 34.5 ± 12.3 nm and consistently distributed pores measuring 107.7 ± 71.4 nm (Fig. S2). The SEM images of the freeze-broken cross-sections of the B-CNF/ISB-PC composites show smooth fracture surfaces without voids, lacking the distinct fibrous texture typical of CNFs. This suggests that ISB-PC was well integrated into the B-CNFs. These morphological observations highlight the dense impregnation and smooth interfaces between ISB-PC and B-CNFs as key contributors to the considerably higher transparency of the B-CNF/ISB-PC composites compared with that of their M-CNF/ISB-PC analogs. In contrast, the M-CNF/ISB-PC composites exhibited rough fracture surfaces and a distinct fibrous texture typical of CNFs. This was attributed to the relatively weak bonding at the interfaces and incomplete impregnation of the M-CNF layer with ISB-PC. Despite the slightly higher inhomogeneity of the M-CNF/ISB-PC composites over the B-CNF/ISB-PC composites, the former showed improved transparency and mechanical properties compared to the M-CNF films; therefore, it can be inferred that the M-CNF/ISB-PC composites also possess favorable dispersion and adhesion between the matrix and polymer.

Surface mechanical properties and durability for glazing plastics

To apply glazing plastics, it is crucial to evaluate the mechanical properties and resistance of the surface to moisture and UV exposure. Pencil hardness tests were conducted to assess the scratch resistances of the composite sheets. M-CNF-1 and ISB-PC exhibited an identical HB-level, one grade higher than BPA-PC's B level. In addition, nanoindentation analysis of M-CNF-1's surface mechanical properties revealed a 4.1-fold increase in indentation hardness (HIT) to 380 ± 30 MPa, and a 22-fold increase in indentation modulus (EIT) to 1.8 ± 0.1 GPa compared to neat plastic (ISB-PC; HIT = 93 ± 20 MPa, and EIT = 0.080 ± 0.018 GPa) as shown in Fig. 5a. Based on the actual Young's modulus values of M-CNF-1 (6.3 GPa) and ISB-PC (3.6 GPa), as presented in Table S1, the EIT value of the composite significantly surpassed that of neat plastic. This substantial

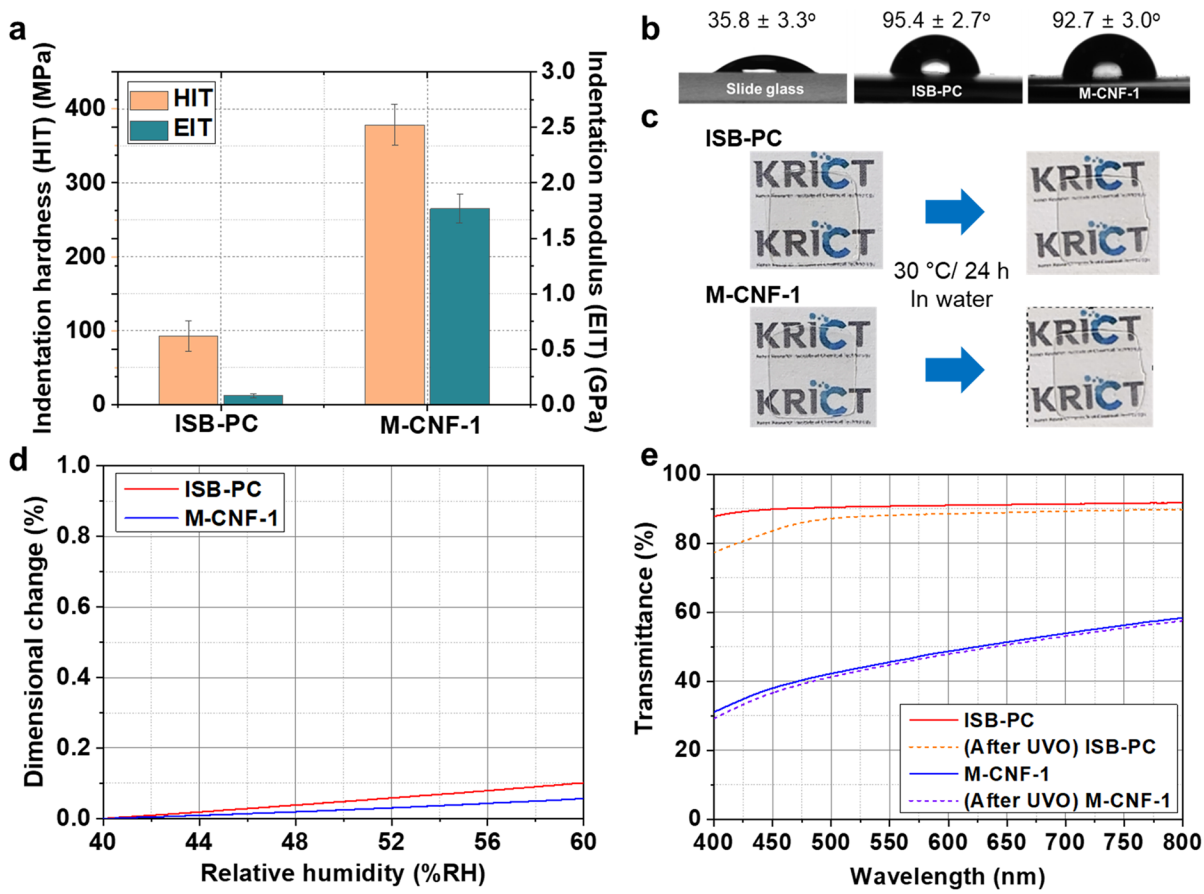

Fig. 5 Surface mechanical properties and durability against water and UV-light. **a** Indentation hardness (HIT) and indentation modulus (EIT) values and **b** Water-contact angles of ISB-PC and M-CNF-1. Water-resistance experiments including **c** Visual (sheet size: 1 cm × 1 cm) and **d** Dimensional changes before and after the immersion of ISB-PC and M-CNF-1 in water. **e** Visible ray transmittance before and after UVO-exposure of ISB-PC and M-CNF-1

difference was theoretically attributed to the incorporation of stiff nanofibers (possessing Young's moduli ranging from 100 to 130 GPa) on the composite sheet surface, which dramatically influences its surface mechanical properties (Dufresne 2013).

Given the high hygroscopicity of ISB, ISB-PC was assumed to exhibit hydrophilic properties. However, owing to the chemical transformation of the hydroxyl groups of ISB monomers to carbonate linkages in polymer chains, the water-contact angle (95.4 ± 2.7°) significantly surpassed that of slide glass (35.8 ± 3.3°), indicating increased hydrophobicity (Fig. 5b). Similarly, in M-CNF-1, where the weight fraction of ISB-PC exceeded 80%, the water-contact angle (92.7 ± 3.0°) further substantiated its hydrophobicity. The water resistance behavior was additionally scrutinized via 24 h-immersion testing in distilled water at 30 °C, yielding no observable alterations in the film's appearance or weight (Fig. 5c). Moreover, dimensional changes of the tested samples exposed to a relative humidity in the range 40–60% were measured as less than 0.1%, and the change in M-CNF-1 was half that of ISB-PC, owing to the presence of nanofibers inside the composite (Fig. 5d). These results verify the composites' outstanding moisture resistance for daily applications.

For the anti-UV aging assessment, samples underwent exposure to 184/254 nm and 26 MW/cm^2 irradiation within a UVO chamber for 30 min at 30 °C. After exposure, no discernible changes in film transparency were observed (Fig. 5e). This resilience to UVO was attributed to the absence of aromatic

groups in the ISB-PC and M-CNF-1 samples, further underscoring their durability (Lai et al. 2019).

The glazing plastics market for the automotive industry is projected to grow at a compound annual growth rate of 8.3%, reaching a market size of US$ 1.6 billion by 2031; this is driven by the increased demand for lightweighting due to the rising production of electric vehicles (Hotaka et al. 2019). Polycarbonate is the primary commercially used resin. Because B-CNFs and ISB-PC are already commercially available materials, any additional cost implications are projected to be minimal. Further technological advancements aimed at enhancing the transparency and dimensional stability of these materials are expected to broaden their commercial applications.

Composting degradation of composite films

A composting experiment was conducted to observe the decomposition behavior of the B-CNF/ISB-PC composite films prepared using the impregnation method (Fig. 6). Composting is an efficient biodegradation method that ensures improved waste management and economic effectiveness, because compostable materials are efficiently biodegraded under composting conditions (Ayilara et al. 2020; Thanh et al. 2022). The composting experiment was performed over 36 weeks under a relative humidity of 60% and temperature of 50–60 °C. The film buried in the compost was removed every three weeks to measure weight loss and verify the degree of decomposition. Over 57% of the B-CNF film, mostly composed of cellulose (negative control sample), started to decompose after three weeks, and decomposed completely after six weeks. In contrast, neither the ISB-PC nor B-CNF-1 films showed any signs of decomposition over the entire 36-week span. It was ultimately determined that by impregnating non-degradable ISB-PC with degradable B-CNFs, the empty spaces in the B-CNFs

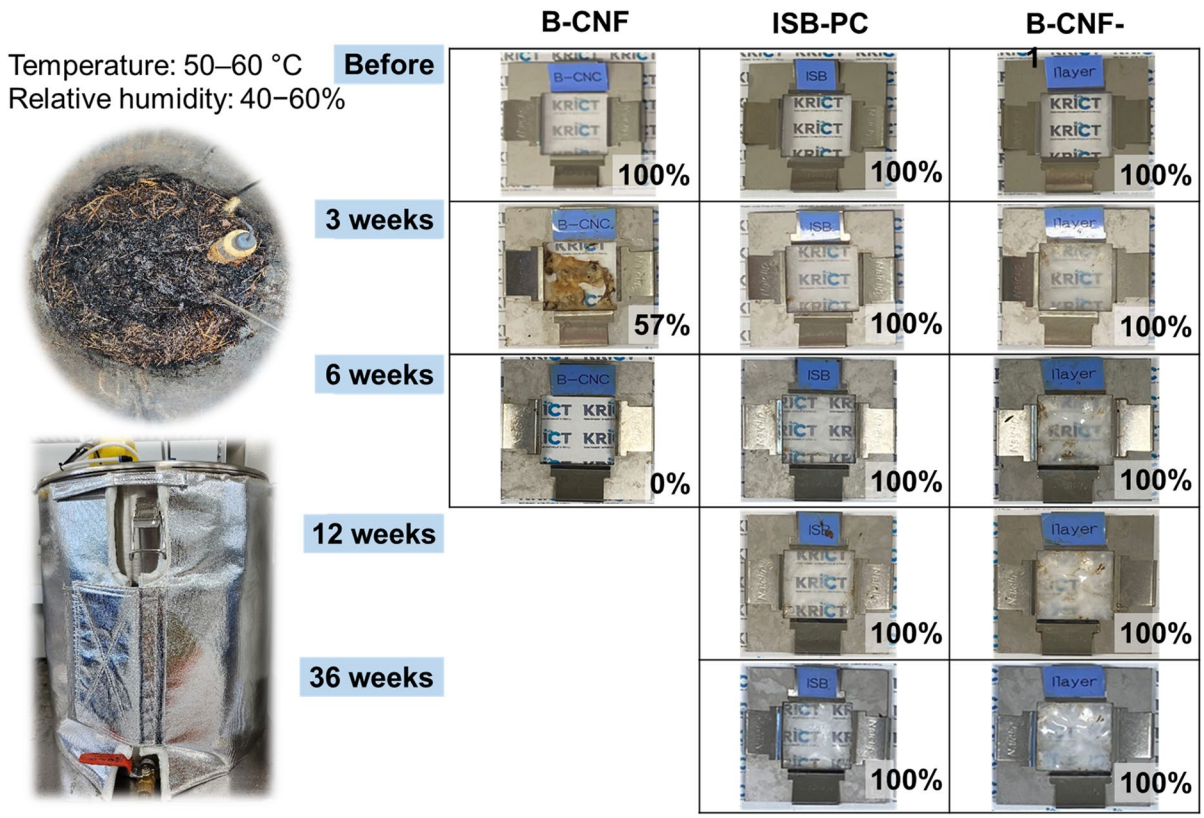

Fig. 6 Optical images of films (3 × 3 cm) during composting degradation experiments

were filled, thus imparting the B-CNF/ISB-PC composites with nondegradable characteristics.

Conclusion

This study marks a notable advancement in the development of a new transparent composite material derived from biomass, specifically, CNFs and ISB-PC. The material is a potential sustainable alternative to conventional glass for various industrial-grade applications, including the automotive and construction sectors (Fig. 7). An impregnation method was employed to combine the CNF film with the ISB-PC, yielding a transparent glazing plastic able to function as a stable solid with high carbon content. When used as a semi-permanent structural element, it contributes to carbon sequestration and has the potential to mitigate the adverse effects of climate change.

The resulting composite materials, particularly M-CNF-1, exhibited improved light transmittance and thermal properties, balancing the performance aspects of neat CNFs and ISB-PC. The mechanical properties of M-CNF-1 are superior to those of conventional materials, such as BPA-PC, which are conventionally used as glass substitutes in structures such as aquariums. Additionally, the B-CNF/ISB-PC composite films displayed higher light transmittance than their M-CNF/ISB-PC equivalents, stemming from the difference in nanofiber disintegration in the B-CNF and M-CNF precursors.

Further, the thermal and dimensional stabilities and morphologies of the composite films underscore their notable potential as viable glass replacements, as evidenced by their remarkably low CTEs, mirroring that of glass. The multilayered B-CNF/ISB-PC sheets displayed the most remarkable properties, owing to the dense impregnation and smooth interfaces between the ISB-PC and B-CNFs, which endowed them with high transparency and remarkable thermal stability even at high temperatures. More importantly, the CNF/ISB-PC composites showcased high dimensional stability even at temperatures as high as 120 °C. Moreover, the CNF/ISB-PC composites demonstrated remarkable consistency in appearance throughout a 32-week long composting test conducted at 58 °C, underscoring their potential for stable long-term use in various applications.

By leveraging the hierarchical wood structure and advantageous properties of CNFs and ISB-PCs, we emphasize the potential of these composites as environmentally friendly alternatives to conventional glass in construction and transportation industries. Furthermore, our study addresses the challenges posed by climate change and presents an innovative pathway for reducing carbon emissions through novel material design. Future analyses should delve deeper into the carbon sequestration potential of CNF/ISB-PC composites, particularly from an LCA standpoint, accounting for energy consumption and carbon emissions during production.

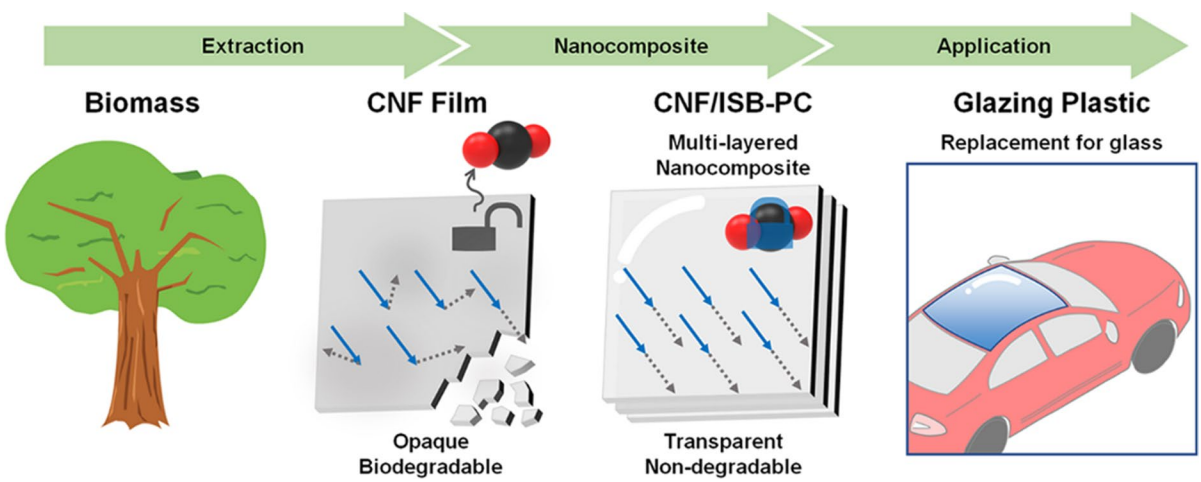

Fig. 7 Transformation of biomass-based CNF films into nanocomposites suitable for use in glazing plastic applications

Acknowledgments We extend our gratitude to Prof. Sejin Choi of Pusan National University for calculating the fiber diameters.

Author contributions SAP: Conceptualization, validation, data curation, writing, and original draft. HJ: Validation, data curation, and formal analysis. MJ: Formal analysis, writing, reviewing, and editing. SK: Formal analysis, writing, reviewing, and editing. SYH: Formal analysis. CHH: Validation and Funding Acquisition. JMK: Formal analysis. DXO: Data curation, writing, review, editing, and supervision. JP: Conceptualization, visualization, formal analysis, writing—review and editing, and supervision.

Funding This work was supported by the Hyundai Motor Company (IIT19-31) and the Korea Research Institute of Chemical Technology (KRICT) core project (KS2442-10). D.X.O. acknowledges the support from the National Research Foundation of Korea (NRF) funded by the Ministry of Science, ICT, and Future Planning (2022M3H4A1A03076577). J.P. acknowledges the support from the National Research Foundation of Korea (NRF), funded by the Ministry of Science and ICT (2015M3D3A1A01064926).

Data availability Data are available upon reasonable request.

Declarations

Conflict of interest The authors declare they have no competing or financial interests.

Consent for publication All authors have given approval to the final version of the manuscript.

Ethical approval All the authors state that they adhere to the Ethical Responsibilities of Authors. In addition, this article does not contain any studies with human participants or animals performed by any of the authors.

References

Arora V, Saran RK, Kumar R, Yadav S (2019) Separation and sequestration of CO_2 in geological formations. Mater Sci Energy Technol 2:647–656. https://doi.org/10.1016/j.mset.2019.08.006

Ayilara M, Olanrewaju O, Babalola O, Odeyemi O (2020) Waste management through composting: challenges and potentials. Sustainability 12:4456. https://doi.org/10.3390/su12114456

Becattini V, Gabrielli P, Mazzotti M (2021) Role of carbon capture, storage, and utilization to enable a net-zero-CO_2-emissions aviation sector. Ind Eng Chem Res 60:6848–6862. https://doi.org/10.1021/acs.iecr.0c05392

Benavides PT, Lee U, Zarè-Mehrjerdi O (2020) Life cycle greenhouse gas emissions and energy use of polylactic acid, bio-derived polyethylene, and fossil-derived polyethylene. J Clean Prod 277:124010. https://doi.org/10.1016/j.jclepro.2020.124010

Bogdanov B, Markovska I, Hristov Y, Georgiev D (2011) Synthesis and properties of glass ceramics of the system Li_2O–Al_2O_3–SiO_2–B_2O_3–P_2O_5. J Balk Tribol Assoc 17:48–55. https://www.researchgate.net/publication/289161914_Synthesis_and_properties_of_glass_ceramics_of_the_system_Li_2O-Al2O3-SiO2-B2O_3-P2O5

Ceballos G, Ehrlich PR, Raven PH (2020) Vertebrates on the brink as indicators of biological annihilation and the sixth mass extinction. Proc Natl Acad Sci USA 117:13596–13602. https://doi.org/10.1073/pnas.1922686117

Chauhan V, Kärki T, Varis J (2022) Review of natural fiber-reinforced engineering plastic composites, their applications in the transportation sector and processing techniques. J Thermoplast Compos Mater 35:1169–1209. https://doi.org/10.1177/0892705719889095

Chen H, Mu Y, Hardacre C, Fan X (2020) Integration of membrane separation with nonthermal plasma catalysis: a proof-of-concept for CO_2 capture and utilization. Ind Eng Chem Res 59:8202–8211. https://doi.org/10.1021/acs.iecr.0c01067

Chen S, Liu J, Zhang Q, Teng F, McLellan BC (2022) A critical review on deployment planning and risk analysis of carbon capture, utilization, and storage (CCUS) toward carbon neutrality. Renew Sust Energ Rev 167:112537. https://doi.org/10.1016/j.rser.2022.112537

Choi S, Kim J, Seo E, Jung H, Jeong J-E, Park YI, Kim JC, Lee DW, Kim B-S, Lee S-H (2023) Dual crosslinking polymer networks: correlation between polymer topologies and self-healing efficiency. Polym Chem 14:1184–1194. https://doi.org/10.1039/D3PY00025G

Chung S, Park S-A, Park SB, Kwak H, Oh DX, Hwang DS, Jeon H, Koo JM, Park J (2023) Biobased super engineering plastic nanocomposite of cellulose nanofibers and isosorbide. Polym Degrad Stabil 215:110445. https://doi.org/10.1016/j.polymdegradstab.2023.110445

Cleal CJ, Thomas BA (2005) Palaeozoic tropical rainforests and their effect on global climates: is the past the key to the present? Geobiology 3:13–31. https://doi.org/10.1111/j.1472-4669.2005.00043.x

Czaplicka N, Konopacka-Łyskawa D, Kościelska B, Łapiński M (2020) Effect of selected ammonia escape inhibitors on carbon dioxide capture and utilization via calcium carbonate precipitation. J CO2 Util 42:101298. https://doi.org/10.1016/j.jcou.2020.101298

Czerwinski F (2021) Current trends in automotive lightweighting strategies and materials. Materials 14:6631. https://doi.org/10.3390/ma14216631

Dufresne A (2013) Nanocellulose: a new ageless bionanomaterial. Mater Today 16:220–227. https://doi.org/10.1016/j.mattod.2013.06.004

Furszyfer Del Rio DD, Sovacool BK, Foley AM, Griffiths S, Bazilian M, Kim J, Rooney D (2022) Decarbonizing the ceramics industry: a systematic and critical review of policy options, developments and sociotechnical systems. Renew Sust Energ Rev 157:112081. https://doi.org/10.1016/j.rser.2022.112081

Guan Q-F, Yang H-B, Han Z-M, Ling Z-C, Yu S-H (2020a) An all-natural bioinspired structural material for plastic replacement. Nat Commun 11:5401. https://doi.org/10.1038/s41467-020-19174-1

Guan Q-F, Yang H-B, Han Z-M, Zhou L-C, Zhu Y-B, Ling Z-C, Jiang H-B, Wang P-F, Ma T, Wu H-A, Yu S-H (2020b) Lightweight, tough, and sustainable cellulose nanofiber-derived bulk structural materials with low thermal expansion coefficient. Sci Adv 6:eaaz1114. https://doi.org/10.1126/sciadv.aaz1114

Guan Q-F, Han Z-M, Yang H-B, Ling Z-C, Yu S-H (2021a) Regenerated isotropic wood. Nat. Sci. Rev. 8:nwaa230. https://doi.org/10.1093/nsr/nwaa230

Guan Q-F, Yang H-B, Han Z-M, Ling Z-C, Yang K-P, Yin C-H, Yu S-H (2021b) Plant cellulose nanofiber-derived structural material with high-density reversible interaction networks for plastic substitute. Nano Lett 21:8999–9004. https://doi.org/10.1021/acs.nanolett.1c02315

Guo D, Yang S, Fu F, Li G, Chu F (2022) New strategy for the preparation of ultra-high-strength wood-epoxy polymer composites. Compos Commun 33:101191. https://doi.org/10.1016/j.coco.2022.101191

Gür TM (2022) Carbon dioxide emissions, capture, storage and utilization: review of materials, processes and technologies. Prog Energ Combust 89:100965. https://doi.org/10.1016/j.pecs.2021.100965

Hanif Z, Jeon H, Tran TH, Jegal J, Park S-A, Kim S-M, Park J, Hwang SY, Oh DX (2017) Butanol-mediated oven-drying of nanocellulose with enhanced dehydration rate and aqueous re-dispersion. J Polym Res 25:191. https://doi.org/10.1007/s10965-017-1343-z

Hauenstein O, Rahman MM, Elsayed M, Krause-Rehberg R, Agarwal S, Abetz V, Greiner A (2017) Biobased polycarbonate as a gas separation membrane and "breathing glass" for energy saving applications. Adv Mater Technol 2:1700026. https://doi.org/10.1002/admt.201700026

Hertwich EG (2021) Increased carbon footprint of materials production driven by rise in investments. Nat Geosci 14:151–155. https://doi.org/10.1038/s41561-021-00690-8

Hong WY (2022) A techno-economic review on carbon capture, utilisation and storage systems for achieving a net-zero CO_2 emissions future. Carbon Capture Sci Technol 3:100044. https://doi.org/10.1016/j.ccst.2022.100044

Hotaka T, Kondo F, Niimi R, Togashi F, Morita Y (2019) Industrialization of automotive glazing by polycarbonate and hard-coating. Polym J 51:1249–1263. https://doi.org/10.1038/s41428-019-0240-1

Iossifidis MJM, Garforth L (2022) Reimagining climate futures: reading annihilation. Geoforum 137:248–257. https://doi.org/10.1016/j.geoforum.2021.12.001

Jeon H, Kim M-S, Park SB, Kim S, Lee M, Park S-A, Hwang SY, Koo JM, Oh DX, Park J (2023) Improved mechanical properties of biodegradable polycaprolactone nanocomposites prepared using cellulose nanocrystals. Cellulose. https://doi.org/10.1007/s10570-023-05615-9

Ji S, Hyun BG, Kim K, Lee SY, Kim S-H, Kim J-Y, Song MH, Park J-U (2016) Photo-patternable and transparent films using cellulose nanofibers for stretchable origami electronics. NPG Asia Mater 8:e299–e299. https://doi.org/10.1038/am.2016.113

Jo YJ (2013) Manufacturing method of cosmetic biocellulose sheet and cosmetic biocellulose sheet by using therof. KR101385501B1

Jung H, Shin G, Kwak H, Hao LT, Jegal J, Kim HJ, Jeon H, Park J, Oh DX (2023) Review of polymer technologies for improving the recycling and upcycling efficiency of plastic waste. Chemosphere 320:138089. https://doi.org/10.1016/j.chemosphere.2023.138089

Kenrick P, Crane PR (1997) The origin and early evolution of plants on land. Nature 389:33–39. https://doi.org/10.1038/37918

Kim JY, Shin EJ, Eom IY, Won K, Kim YH, Choi D, Choi IG, Choi JW (2011) Structural features of lignin macromolecules extracted with ionic liquid from poplar wood. Biores Technol 102:9020–9025. https://doi.org/10.1016/j.biortech.2011.07.081

Kim J-K, Choi B, Jin J (2020) Transparent, water-stable, cellulose nanofiber-based packaging film with a low oxygen permeability. Carbohydr Polym 249:116823. https://doi.org/10.1016/j.carbpol.2020.116823

Kim H, Jeon H, Shin G, Lee M, Jegal J, Hwang SY, Oh DX, Koo JM, Eom Y, Park J (2021a) Biodegradable nanocomposite of poly(ester-co-carbonate) and cellulose nanocrystals for tough tear-resistant disposable bags. Green Chem 23:2293–2299. https://doi.org/10.1039/D0GC04072J

Kim H, Shin MS, Jeon H, Koo JM, Eom Y, Choi S, Shin G, Oh DX, Hwang SY, Park J (2021b) Highly reinforced poly(butylene succinate) nanocomposites prepared from chitosan nanowhiskers by in-situ polymerization. Int J Biol Macromol 173:128–135. https://doi.org/10.1016/j.ijbiomac.2021.01.102

Koo JM, Kang J, Shin S-H, Jegal J, Cha HG, Choy S, Hakkarainen M, Park J, Oh DX, Hwang SY (2020) Biobased thermoplastic elastomer with seamless 3D-printability and superior mechanical properties empowered by in-situ polymerization in the presence of nanocellulose. Compos Sci Technol 185:107885. https://doi.org/10.1016/j.compscitech.2019.107885

Kucherov FA, Gordeev EG, Kashin AS, Ananikov VP (2017) Three-dimensional printing with biomass-derived PEF for carbon-neutral manufacturing. Angew Chem Int Ed 56:15931–15935. https://doi.org/10.1002/anie.201708528

Labaran YH, Mathur VS, Muhammad SU, Musa AA (2022) Carbon footprint management: a review of construction industry. Clean Eng Technol 9:100531. https://doi.org/10.1016/j.clet.2022.100531

Lai W, Su L, Zhang M, Yan J, Wu G (2019) Tuning the optical clarity of glass fiber-reinforced polycarbonates by reactive blending with alternatives from biorenewable isosorbide. J Polym Sci Part a: Polym Chem 57:1670–1681. https://doi.org/10.1002/pola.29432

Lee K-Y, Aitomäki Y, Berglund LA, Oksman K, Bismarck A (2014) On the use of nanocellulose as reinforcement in polymer matrix composites. Compos Sci Technol 105:15–27. https://doi.org/10.1016/j.compscitech.2014.08.032

Leonzio G, Bogle D, Foscolo PU, Zondervan E (2020) Optimization of CCUS supply chains in the UK: A strategic role for emissions reduction. Chem Eng Res Des 155:211–228. https://doi.org/10.1016/j.cherd.2020.01.002

Li J, Nawaz H, Wu J, Zhang J, Wan J, Mi Q, Yu J, Zhang J (2018) All-cellulose composites based on the self-reinforced effect. Compos Commun 9:42–53. https://doi.org/10.1016/j.coco.2018.04.008

Lim AY, Park SB, Choi Y, Oh DX, Park J, Jeon H, Koo JM (2023) Extending the high-performing boundaries of a fully bio-based thermal shrinkage film targeted for food

packaging applications. Green Chem 25:9711–9719. https://doi.org/10.1039/D3GC02193A

Lindsey R, Dahlman L (2023) Climate change: global temperature. National Oceanic and Atmospheric Administration. https://www.climate.gov/news-features/understanding-climate/climate-change-global-temperature. Accessed 27 Nov 2023

Liu Z, Deng Z, Davis SJ, Giron C, Ciais P (2022) Monitoring global carbon emissions in 2021. Nat Rev Earth Environ 3:217–219. https://doi.org/10.1038/s43017-022-00285-w

Ludwicka K, Kaczmarek M, Białkowska A (2020) Bacterial nanocellulose—a biobased polymer for active and intelligent food packaging applications: Recent advances and developments. Polymers 12:2209. https://doi.org/10.3390/polym12102209

Majumdar A, Deutch J (2018) Research opportunities for CO_2 utilization and negative emissions at the gigatonne scale. Joule 2:805–809. https://doi.org/10.1016/j.joule.2018.04.018

Marocco Stuardi F, MacPherson F, Leclaire J (2019) Integrated CO_2 capture and utilization: A priority research direction. Curr Opin Green Sustain Chem 16:71–76. https://doi.org/10.1016/j.cogsc.2019.02.003

Motagamwala AH, Won W, Sener C, Alonso DM, Maravelias CT, Dumesic JA (2018) Toward biomass-derived renewable plastics: production of 2,5-furandicarboxylic acid from fructose. Sci Adv 4:eaap9722. https://doi.org/10.1126/sciadv.aap9722

Nguyen H-L, Tran TH, Hao LT, Jeon H, Koo JM, Shin G, Hwang DS, Hwang SY, Park J, Oh DX (2021) Biorenewable, transparent, and oxygen/moisture barrier nanocellulose/nanochitin-based coating on polypropylene for food packaging applications. Carbohydr Polym 271:118421. https://doi.org/10.1016/j.carbpol.2021.118421

Nogi M, Yano H (2008) Transparent nanocomposites based on cellulose produced by bacteria offer potential innovation in the electronics device industry. Adv Mater 20:1849–1852. https://doi.org/10.1002/adma.200702559

Park S-A, Choi J, Ju S, Jegal J, Lee KM, Hwang SY, Oh DX, Park J (2017) Copolycarbonates of bio-based rigid isosorbide and flexible 1,4-cyclohexanedimethanol: merits over bisphenol-a based polycarbonates. Polymer 116:153–159. https://doi.org/10.1016/j.polymer.2017.03.077

Park S-A, Eom Y, Jeon H, Koo JM, Lee ES, Jegal J, Hwang SY, Oh DX, Park J (2019a) Preparation of synergistically reinforced transparent bio-polycarbonate nanocomposites with highly dispersed cellulose nanocrystals. Green Chem 21:5212–5221. https://doi.org/10.1039/c9gc02253h

Park S-A, Jeon H, Kim H, Shin S-H, Choy S, Hwang DS, Koo JM, Jegal J, Hwang SY, Park J, Oh DX (2019b) Sustainable and recyclable super engineering thermoplastic from biorenewable monomer. Nat Commun 10:2601. https://doi.org/10.1038/s41467-019-10582-6

Pashazadeh S, Ghanbari R, Bek M, Aulova A, Moberg T, Brolin A, Kádár R (2023) Mapping surface defects in highly-filled wood fiber polymer composite extrusion from inline spectral analysis. Compos Sci Technol 242:110133. https://doi.org/10.1016/j.compscitech.2023.110133

Pfister M, Belaissaoui B, Favre E (2017) Membrane gas separation processes from wet postcombustion flue gases for carbon capture and use: a critical reassessment. Ind Eng Chem Res 56:591–602. https://doi.org/10.1021/acs.iecr.6b03969

Prevost L (2023) Colleges showcase mass timber, in research and on display. The New York Times. https://www.nytimes.com/2023/03/14/business/mass-timber-universities.html. Accessed 27 Nov 2023

Qi Y, Guo Y, Liza AA, Yang G, Sipponen MH, Guo J, Li H (2023) Nanocellulose: a review on preparation routes and applications in functional materials. Cellulose 30:4115–4147. https://doi.org/10.1007/s10570-023-05169-w

Qian H, Liu J, Wang X, Pei W, Fu C, Ma M, Huang C (2023) The state-of-the-art application of functional bacterial cellulose-based materials in biomedical fields. Carbohydr Polym 300:120252. https://doi.org/10.1016/j.carbpol.2022.120252

Quarton CJ, Samsatli S (2020) The value of hydrogen and carbon capture, storage and utilisation in decarbonising energy: insights from integrated value chain optimisation. Appl Energ 257:113936. https://doi.org/10.1016/j.apenergy.2019.113936

Ra EC, Kim KY, Kim EH, Lee H, An K, Lee JS (2020) Recycling carbon dioxide through catalytic hydrogenation: Recent key developments and perspectives. ACS Catal 10:11318–11345. https://doi.org/10.1021/acscatal.0c02930

Raabe D (2023) The materials science behind sustainable metals and alloys. Chem Rev 123:2436–2608. https://doi.org/10.1021/acs.chemrev.2c00799

Ramage MH, Burridge H, Busse-Wicher M, Fereday G, Reynolds T, Shah DU, Wu G, Yu L, Fleming P, Densley-Tingley D, Allwood J, Dupree P, Linden PF, Scherman O (2017) The wood from the trees: the use of timber in construction. Renew Sust Energ Rev 68:333–359. https://doi.org/10.1016/j.rser.2016.09.107

Ren L, Zhou S, Peng T, Ou X (2021) A review of CO_2 emissions reduction technologies and low-carbon development in the iron and steel industry focusing on China. Renew Sust Energ Rev 143:110846. https://doi.org/10.1016/j.rser.2021.110846

Solikhin A, Syamani FA, Hastati DY, Budiman I, Purnawati R, Mubarok M, Yanti H, Fachruddin A, Saad S, Jaenab S, Badrudin U, Kurniawan T (2023) Review on lignocellulose valorization for nanocarbon and its composites: Starting from laboratory studies to business application. Int J Biol Macromol 239:124082. https://doi.org/10.1016/j.ijbiomac.2023.124082

Song Y, Jun S, Na Y, Kim K, Jang Y, Wang J (2023) Geomechanical challenges during geological CO_2 storage: a review. Chem Eng J 456:140968. https://doi.org/10.1016/j.cej.2022.140968

Stegmann P, Daioglou V, Londo M, van Vuuren DP, Junginger M (2022) Plastic futures and their CO_2 emissions. Nature 612:272–276. https://doi.org/10.1038/s41586-022-05422-5

Tanpichai S, Boonmahitthisud A, Soykeabkaew N, Ongthip L (2022) Review of the recent developments in all-cellulose nanocomposites: properties and applications. Carbohydr Polym 286:119192. https://doi.org/10.1016/j.carbpol.2022.119192

Thanh TV, Hao LT, Cho H-Y, Kim H, Park S-A, Lee M, Kim HJ, Jeon H, Hwang SY, Park J, Oh DX, Koo JM (2022)

Sustainable poly(butylene adipate-co-furanoate) composites with sulfated chitin nanowhiskers: synergy leading to superior robustness and improved biodegradation. ACS Sustain Chem Eng 10:8411–8422. https://doi.org/10.1021/acssuschemeng.2c01395

Vanderbilt T (2017) The school prepping for apocalypse. The New York Times. https://www.nytimes.com/2017/11/13/t-magazine/bali-green-school.html. Accessed 27 Nov 2023

Vanderreydt I, Rommens T, Tenhunen-Lunkka A, Mortensen LF, Tange I (2021) Greenhouse gas emissions and natural capital implications of plastics (including biobased plastics). EEA report. European Environment Agency (EAA)

Vaz S, Rodrigues de Souza AP, Lobo Baeta BE (2022) Technologies for carbon dioxide capture: a review applied to energy sectors. Clean Eng Technol 8:100456. https://doi.org/10.1016/j.clet.2022.100456

Vieira MGA, da Silva MA, dos Santos LO, Beppu MM (2011) Natural-based plasticizers and biopolymer films: a review. Eur Polym J 47:254–263. https://doi.org/10.1016/j.eurpolymj.2010.12.011

Wang F, Harindintwali JD, Yuan Z, Wang M, Wang F, Li S, Yin Z, Huang L, Fu Y, Li L, Chang SX, Zhang L, Rinklebe J, Yuan Z, Zhu Q, Xiang L, Tsang DCW, Xu L, Jiang X, Liu J, Wei N, Kastner M, Zou Y, Ok YS, Shen J, Peng D, Zhang W, Barcelo D, Zhou Y, Bai Z, Li B, Zhang B, Wei K, Cao H, Tan Z, Zhao LB, He X, Zheng J, Bolan N, Liu X, Huang C, Dietmann S, Luo M, Sun N, Gong J, Gong Y, Brahushi F, Zhang T, Xiao C, Li X, Chen W, Jiao N, Lehmann J, Zhu YG, Jin H, Schaffer A, Tiedje JM, Chen JM (2021) Technologies and perspectives for achieving carbon neutrality. The Innovation 2:100180. https://doi.org/10.1016/j.xinn.2021.100180

Wu Z, Jiang Y, Li Z, Wang B, Wang H, Chen S (2021) Bacterial cellulose nanofiber distribution on gelatin and silk fibroin scaffolds and the cell behavior. Cellulose 28:91–102. https://doi.org/10.1007/s10570-020-03545-4

Xu J, Sahu S, Cao L, Anilkumar P, Tackett KN II, Qian H, Bunker CE, Guliants EA, Parenzan A, Sun Y-P (2011) Carbon nanoparticles as chromophores for photon harvesting and photoconversion. ChemPhysChem 12:3604–3608. https://doi.org/10.1002/cphc.201100640

Yano H, Omura H, Honma Y, Okumura H, Sano H, Nakatsubo F (2018) Designing cellulose nanofiber surface for high density polyethylene reinforcement. Cellulose 25:3351–3362. https://doi.org/10.1007/s10570-018-1787-2

Zhang X, Jiao K, Zhang J, Guo Z (2021) A review on low carbon emissions projects of steel industry in the World. J Clean Prod 306:127259. https://doi.org/10.1016/j.jclepro.2021.127259

Zhang H, Hu Q, Si T, Tang X, Shan S, Gao X, Peng L, Chen K (2023) All-cellulose air filter composed with regenerated nanocellulose prepared through a facile method with shear-induced. Int J Biol Macromol 228:548–558. https://doi.org/10.1016/j.ijbiomac.2022.11.095

Zhu M, Fan B (2021) Exploring the relationship between rising temperatures and the number of climate-related natural disasters in China. Int J Environ Res Public Health 18:745. https://doi.org/10.3390/ijerph18020745